Langmuir
Article
pubs.acs.org/Langmuir


# Capillary Filling in Nanostructured Porous Silicon

Leandro N. Acquaroli,*[,†] Raúl Urteaga,[†,§] Claudio L. A. Berli,[‡] and Roberto R. Koropecki[†,§]

[†]*Grupo de Física de Semiconductores,* [‡]*Microfluídica, INTEC (UNL-CONICET), Güemes 3450, 3000 Santa Fe, Argentina, and* [§]*Facultad de Ingeniería Química (UNL), Santiago del Estero 2829, 3000 Santa Fe, Argentina*

*Received November 11, 2010. Revised Manuscript Received December 21, 2010*

An experimental study on the capillary filling of nanoporous silicon with different fluids is presented. Thin nanoporous membranes were obtained by electrochemical anodization, and the filling dynamics was measured by laser interferometry, taking advantage of the optical properties of the system, related with the small pore radius in comparison to light wavelength. This optical technique is relatively simple to implement and yields highly reproducible data. A fluid dynamic model for the filling process is also proposed including the main characteristics of the porous matrix (tortuosity, average hydraulic radius). The model was tested for different ambient pressures, porous layer morphology, and fluid properties. It was found that the model reproduces well the experimental data according to the different conditions. The predicted pore radii quantitatively agree with the image information from scanning electron microscopy. This technique can be readily used as nanofluidic sensor to determine fluid properties such as viscosity and surface tension of a small sample of liquid. Besides, the whole method can be suitable to characterize a porous matrix.

## Introduction

Nanostructured porous materials provide attractive functionalities to be used in fundamental studies as well as in novel applications such as biological[1] and chemical[2] sensing. In particular, since pore radii are comparable to the molecular size of large biomolecules (DNA, proteins), silicon membranes are of interest as nanofluidic components in lab-on-a-chip technology.[3−5]

The spontaneous filling of nanochannels driven by capillary forces is an attractive strategy to transport fluids without external pumps. For this purpose, understanding and controlling the fluid dynamics is of primary importance. In fact, although capillary filling has been known for many years, there is a renewed interest on the subject at present, mainly due to the advent of nanofluidic devices.[6−11]

Previous works employing optical techniques to measure capillary imbibition make use of microscopy photography[12] and miniaturized Fabry-Pérot interferometers.[13,14] These methods are suitable to analyze single nanochannels in a lateral view configuration.

In this Article, we present an experimental study on the capillary filling of nanoporous silicon films with different fluids, ambient pressures, and porous matrix morphology. Since pore radius is small compared to light wavelength, the thickness of the layers can be measured by laser interferometry along the fluid flow direction.

Thin films of nanostructured porous silicon (PS) can be fabricated by electrochemical anodization of doped crystalline silicon (c-Si) wafers in a hydrofluoric solution. As a result, a porous net grows inside the c-Si wafer with pore sizes varying from 2 nm up to 10 $\mu$m depending on the resistivity of the c-Si, electrolyte composition, and preparation conditions.[15] The porosity and pore size of PS can be controlled by the current density used, and a time dependent profile in the current density results in a profile of porosities.[15] With a pulse of sufficiently large current density (electropolishing current), it is possible to separate the porous layer from the c-Si substrate. If glass is used to support the porous layer, the capillary forces upon drying result in a strong adherence of the film onto the glass.[16]

Attaining a quantitative description of the filling dynamics is also a main objective of this work. Calculations were carried out in the context of the hydrodynamic approach, where the classical Lucas−Washburn[17,18] description was modified to account for the main characteristics of the porous matrix (tortuosity, average hydraulic radius) and the pressure of entrapped air (channel ends in contact with the supporting substrate are closed).

The paper is organized as follows: the next section presents the fabrication of silicon membranes and the experiments conducted to study dynamics of capillary filling. The theoretical section describes the basis of optical measurements and the governing equations of the fluid dynamic problem. Then experimental

*To whom correspondence should be addressed. Mailing address: Instituto de Desarrollo Tecnológico para la Industria Química, UNL - CONICET, Güemes 3450, 3000 Santa Fe, Argentina. Telephone: +54 0342 455 9174. E-mail: lnacquaroli@santafe-conicet.gov.ar.

(1) Rossi, A. M.; Wang, L.; Reipa, V.; Murphya, T. E. *Biosens. Bioelectron.* **2007**, *23*, 741.
(2) Acquaroli, L. N.; Urteaga, R.; Koropecki, R. R. *Sens. Actuators, B* **2010**, *149*, 189.
(3) Eijkel, J. C. T.; van den Berg, A. *Microfluid. Nanofluid.* **2005**, *1*, 249.
(4) van den Berg, A.; Wessling, M. *Nature* **2007**, *445*, 726.
(5) Kovarik, M. L.; Jacobson, S. C. *Anal. Chem.* **2009**, *81*, 7133.
(6) Han, A.; Mondin, G.; Hegelbach, N. G.; de Rooij, N. F.; Staufer, U. *J. Colloid Interface Sci.* **2006**, *293*, 151.
(7) Haneveld, J.; Tas, N. R.; Brunets, N.; Jansen, H. V.; Elwenspoek, M. *J. Appl. Phys.* **2008**, *104*, 014309.
(8) Gruener, S.; Hofmann, T.; Wallacher, D.; Kityk, A. V.; Huber, P. *Phys. Rev. E* **2009**, *79*, 067301.
(9) Phan, V. N.; Nguyen, N. T.; Yang, C.; Joseph, P.; Djeghlaf, L.; Bourrier, D.; Gue, A. M. *Langmuir* **2010**, *26*, 13251.
(10) Radiom, M.; Chan, W. K.; Yang, C. *Microfluid. Nanofluid.* **2010**, *9*, 65.
(11) Abgrall, P.; Nguyen, N. T. *Anal. Chem.* **2008**, *80*, 7.
(12) Kusumaatmaja, H.; Pooley, C. M.; Girardo, S.; Pisignano, D.; Yeomans, J. M. *Phys. Rev. E* **2008**, *77*, 067301.
(13) van Delft, K. M.; Eijkel, J. C. T.; Mijatovic, D.; Druzhinina, T. S.; Rathgen, H.; Tas, N. R.; van den Berg, A.; Mugele, F. *Nano Lett.* **2007**, *7*, 345.
(14) Oh, J. M.; Faez, T.; de Beer, S.; Mugele, F. *Microfluid. Nanofluid.* **2010**, *9*, 123.
(15) Zhang, G. X. In *Modern Aspects of Electrochemistry*; Vayenas, C. G., White, R. E., Gamboa-Adelco, M. E., Eds.; Springer: New York, 2006; pp 65−133.
(16) Bisi, O.; Ossicini, E.; Pavesi, L. *Surf. Sci. Rep.* **2000**, *38*, 1.
(17) Lucas, R. *Kolloid-Z.* **1918**, *23*, 15.
(18) Washburn, E. W. *Phys. Rev.* **1921**, *17*, 273.

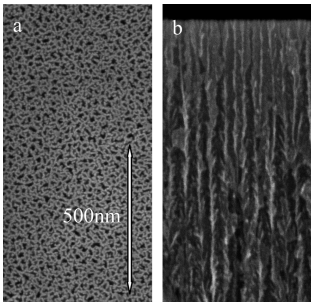


**Figure 1.** SEM images showing the morphology of a PS layer fabricated at 25 mA/cm$^2$: (a) frontal view and (b) lateral view. The scale is the same for both images.

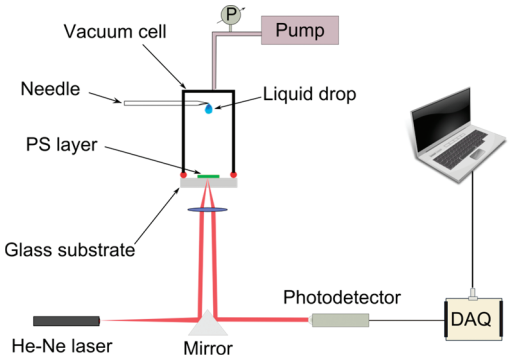


**Figure 2.** Schematic diagram of the experimental setup. A liquid drop impinges upon the porous layer, and the fluid penetrates the porous matrix by capillary forces. The reflectance progress is measured from the back side of the layer at 48 kHz. The air pressure in the chamber is controlled with a peristaltic pump.

results are discussed in terms of the proposed model. Finally, the main conclusions are outlined.

## Materials and Methods

**Porous Silicon Preparation.** Porous silicon (PS) layers of about 15 $\mu$m thick were fabricated by electrochemical anodization of p-type boron doped c-Si wafers (resistivity 1−4 m$\Omega\cdot$cm, orientation ⟨100⟩) in a HF (50%)/EtOH solution with proportions 1:2 (v:v). The electrochemical cell is a Teflon beaker where the Si wafer acts as the anode and the cathode is formed by a platinum wire. Using this cell, PS is formed on the wafer surface exposed to HF.[15]

Each layer was prepared at a constant current density within a range from 5 to 40 mA/cm$^2$ in galvanostatic mode. The porosity of these films varies between 55% and 75%, with pore sizes ranging from 5 to 20 nm, respectively (the pore radii distribution resulting for each current density is discussed in the Pore Size section; see also Figure 8).

After fabrication, an electropolishing current density of about 100 mA/cm$^2$ in a HF (50%)/EtOH solution with proportions 1:7 (v:v) was applied to remove PS layers from the c-Si substrate, and the layers were transferred over 1 mm thick glass substrates.

The thicknesses of the films were measured by using optical microscopy, and scanning electron microscopy (SEM) images were also taken to characterize the PS layers, as shown in Figure 1. The values of layer porosities were estimated from the measurements of the reflectance spectra[19] in the range of 200−1100 nm.

**Measurement System.** Figure 2 shows the system used to measure ligth reflection from PS thin films during liquid imbibition by capillary filling. A monochromatic He−Ne (wavelength 632.8 nm) laser beam was focused on the PS layer from the rear, through the glass substrate, in order to obtain the time response

(19) Theiss, W. *Surf. Sci. Rep.* **1997**, *29*, 91.

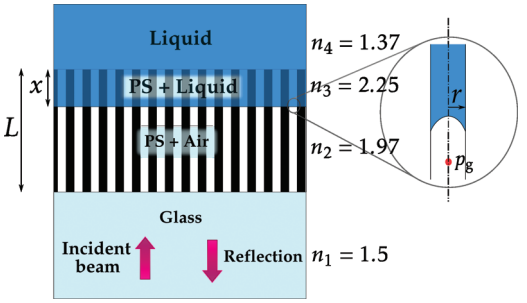


**Figure 3.** Scheme of dielectric layer sequence and the respective refractive indexes $n$. The porous film ($n_2$) is fixed on a glass substrate ($n_1$). The liquid ($n_4$) infiltrates into the porous matrix, leading to an effective refractive index ($n_3$). The $n$ values indicated at the right correspond to isopropyl alcohol ($n_4$), a 60% porosity layer ($n_2$), at $\lambda$ = 632.8 nm.

reflectance. A liquid drop is released from a needle over the PS layer. The drop impinges upon the porous film, and the fluid (driven by capillary forces) begins to penetrate through the porous net compressing the entrapped air. The light reflected from the PS layer is collected by a photodetector which produces a signal proportional to the reflected light intensity. The time dependent response is measured using a digital adquisition system (DAQ). Data were recorded at 48 kHz by a computer controlled 14 bit acquisition card. The porous film was located in a sealed container where gas pressure was controlled by employing a peristaltic pump over 0.1−2.5 atm (absolute).

## Theoretical Models

**Reflectance Variation upon Flow Imbibition.** In this section, we describe the model that relates the measured reflectance to the position of the advancing front of the fluid in the porous layer. Since the incident light wavelength $\lambda$ used to obtain the reflectance measurements is much greater than the mean pore size, the refractive index of the PS layer can be computed using an effective medium theory.[16,19] As the liquid penetrates into the porous layer, the pores are filled with fluid and the effective refractive index increases. A scheme of the resulting dielectric layers is shown in Figure 3. The incident light reflects in any plane interface, and the total reflected intensity must be calculated as the sum of all contributions.

In this system, three interfaces contribute to the reflection of light. According to Fresnel coefficients, the higher the refractive indexes contrast the stronger the reflection.[20] In Figure 3, the reflection coefficient in the $n_2-n_3$ interface (the moving interface) is at least 4 times smaller than the other two. Furthermore, as this interface is not expected to be perfectly flat, the reflectance in this case will be even lower (a roughness of around 100 nm produces a reduction in the reflected intensity of an order of magnitude[20]). According to these considerations, the reflectance will be dominated by the interference of the reflected beams in the two fixed interfaces.

The optical path of the porous layer of thickness $L$ infiltrated at a distance $x$ can be calculated as $e_0 = n_2(L - x) + n_3 x$. Given that the reflected beam at the $n_3-n_4$ interface travels the layer twice and taking into account a phase shift at the $n_1-n_2$ interface, the total phase shift will be $\Delta\phi = \pi + 4\pi e_0/\lambda$. A constructive interference will occur when $\Delta\phi$ is a multiple of $2\pi$. On the other hand, when $\Delta\phi$ is an odd multiple of $\pi$, there will be a destructive interference. Therefore, as $x$ increases, the reflectance will have an extreme at

(20) Knittl., Z. *Optics of thin films* (*An optical multilayer theory*); John Wiley & Sons: New York, 1976.

any time the phase shift is a multiple of $\pi$, that is, when the optical path $e_0$ is a multiple of $\lambda/4$. In this way, it is possible to correlate the variation of reflectance from one extreme to the next with an increase in the position of infiltration given by $\Delta x = \lambda/[4(n_3 - n_2)]$. In the example of Figure 3, the reflectance is expected to change from one extreme to the next when the liquid penetrates about 560 nm.

Another contribution to the total reflection occurs in the first interface between the air and the glass (not shown in Figure 3). However, since the glass thickness is about 1 mm and not perfectly flat, the reflection on this interface only contributes to the total reflectance with a constant value, approximately equal to 4% of the incident beam intensity.

**Fluid Dynamics Model for a Single Capillary.** Capillary filling is described in the framework of continuum fluid mechanics. The flow is established in the $x$ direction, as shown in Figure 3, and temperature is assumed to be uniform in the entire flow domain. For the sake of clarity, first we consider the filling of a single, idealized cylindrical capillary of radius $r$ and length $L$, with a closed end. The driving force of the filling process is Laplace pressure due to the surface tension $\sigma$ of the liquid, which forms a meniscus at the liquid−gas interface with a contact angle $\theta$ with the wall (zoom in Figure 3). The hydraulic resistance of fluid motion is given by Poiseuille flow, which is valid for incompressible Newtonian fluids of viscosity $\mu$. A fully developed flow is required, which is attained in capillaries of large aspect ratios ($L/r \gg 1$). Although the hydraulic resistance of air is negligible, the compression of entrapped air (closed-end channels) causes an additional resistance. Considering an ideal gas under isothermal conditions, the air back pressure can be included as $p_g = p_0 x/(L - x)$, where $p_0$ is the ambient pressure.

In steady state, the balance of capillary, viscous, and air pressure forces leads to the following expression for the mean fluid velocity $v$ in the capillary:[9,10]

$$v = \frac{1}{8\mu x}\left(2r\sigma\cos\theta - \frac{p_0 r^2 x}{L - x}\right) \tag{1}$$

At the beginning of the process, when $x \ll L$, the model coincides with the classical Lucas−Washburn equation[17,18] for the capillary filling of open channels. On the other hand, eq 1 predicts that fluid velocity vanishes when the pressure of entrapped air equals the Laplace pressure.

This approach is known to provide a suitable description of the filling dynamics in milli- and microchannels. Concerning the fact that the continuum hypothesis is expected to breakdown when fluids are confined to spaces containing relatively few fluid molecules, several recent studies prove the validity of the model in microfabricated nanochannels with heights lower than 10 nm.[6,7,13]

It should be noted that eq 1 describes a quasi-steady state indeed: it is assumed that, at any given time, the velocity profile instantaneously relaxes toward Poiseuille flow. This approximation is accurate if the characteristic time $t_{ch} = \rho r^2/\mu$ is sufficiently low ($\rho$ is the fluid density).[21] In the experiments reported here, $r$ is around 10 nm and hence $t_{ch}$ is on the order $10^{-10}$ s, which is much lower that the temporal resolution limit of our measurements.

Equation 1 also assumes that the contact angle $\theta$ preserves the equilibrium value when the liquid flows. Several attempts to account for the increase of $\theta$ with the fluid velocity (dynamic contact angle) have been reported in the literature (for example, ref 23). For the fluid velocities of our experiments (~1 mm/s), it is found that the increase of $\theta$, over a static value 0°, is lower than 5°, and thus, the possible error in the factor $\cos\theta$ is below 1%.

Absorption of the compressed gas in the liquid is disregarded in this work, since the characteristic diffusion time is about two orders of magnitud greater than filling time.[9]

Molecular dynamics simulation results[22] show that a prewetting layer of molecules propagates into the capillary following the Lucas−Washburn law, which moves more rapidly than the meniscus front (at least in the first stages of the filling). The potential influence of the prewetting on capillary dynamics is not considered in the present model.

Finally, it is worth mentioning that the contribution of hydrostatic pressure is accurately neglected in the present analysis, taking into account that the ratio between gravitational and capillary forces, the so-called Bond number, is $\rho g L r/\sigma \sim 10^{-9}$. This also ensures that the meniscus is hemispherical, with a constant radius of curvature given by $r/\cos\theta$.

**Fluid Dynamics Model for an Assembly of Capillaries.** Equation 1 captures the main features of the filling dynamics in single capillaries; however, it is insufficient to describe the filling of PS films, where a certain distribution of pore sizes and shapes is present (see the images in Figure 8). In addition, pore axes are not aligned in flow direction. In order to account for these effects, as a first approximation, we consider an assembly of parallel capillaries, all of them with the same effective length $L_{eff}$ but different pore perimeter $P$ and cross-sectional area $A$. The concept of hydraulic radius $r_h = 2A/P$ is then required[21] as well as the tortuosity $\tau = L_{eff}/L$, which accounts for local orientation of capillary segments. Under these conditions, the velocity $dx/dt$ of the advancing front ($n_2$−$n_3$ interface in Figure 3) can be expressed as

$$\frac{dx}{dt} = \frac{1}{8\mu\tau^2 x}\left(2\sigma\langle r_h\rangle\cos\theta - p_0\langle r_h^2\rangle\frac{x}{L - x}\right) \tag{2}$$

where $\langle r_h\rangle$ and $\langle r_h{}^2\rangle$ are the area weighted averages of the hydraulic radius and the square hydraulic radius, respectively, as demonstrated in Appendix A.

By introducing dimensionless variables $x^* = x/L$ and $t^* = t/t_{fill}$, eq 2 is rewritten as follows:

$$2\frac{dx^*}{dt^*} = \frac{1}{x^*} - \frac{\alpha}{1 - x^*} \tag{3}$$

where $t_{fill}$ is a characteristic filling time defined as

$$t_{fill} = \frac{2\mu\tau^2 L^2}{\langle r_h\rangle\sigma\cos\theta} \tag{4}$$

and $\alpha$ (dimensionless) is the ratio between ambient pressure and Laplace capillary pressure,

$$\alpha = \frac{\langle r_h{}^2\rangle p_0}{2\langle r_h\rangle\sigma\cos\theta} \tag{5}$$

Analytical integration of eq 3 yields the following implicit function:

$$t^*(x^*) = \frac{(x^*)^2}{(1+\alpha)} - \frac{2\alpha x^*}{(1+\alpha)^2} - \frac{2\alpha}{(1+\alpha)^3}\ln\left[1 - (1+\alpha)x^*\right] \tag{6}$$

It is readily observed that if $\alpha \to 0$, then $x^* \to (t^*)^{1/2}$; that is, when there is no entrapped air, the well-known $t^{1/2}$ dependence of the Lucas−Washburn solution[17,18] is recovered. For arbitrary values of $\alpha$, when $t^* \to \infty$, then $x^* \to 1/(1 + \alpha)$, meaning that the maximum filling length is controlled by the ratio of ambient to Laplace pressures.

(21) White, F. M. *Viscous Fluid Flow*; McGraw-Hill, Inc.: New York, 1974.
(22) Henrich, B.; Cupelli, C.; Santer, M.; Moseler, M. *New J. Phys.* **2008**, *10*, 113022.
(23) Popescu, M. N.; Ralston, J.; Sedev, R. *Langmuir* **2008**, *24*, 12710.

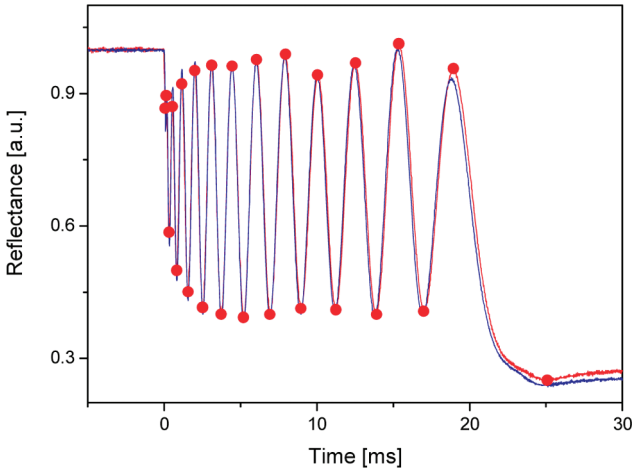


**Figure 4.** Normalized reflectance during the imbibition of a PS layer (15 $\mu$m thick, fabricated using a current density of 13 mA/cm$^2$), with isopropyl alcohol at room temperature and the pressure of 1 atm. Two different measurements are reported to show the repeatability of the experiment. The symbols on the curve indicate the extremes of the reflectance used to obtain the time evolution of the filling fraction.

## Results and Discussion

Figure 4 shows two normalized reflectance measurements at atmospheric pressure during the imbibition of a PS film with isopropyl alcohol. It is observed that reflectance presents oscillations characteristic of an interference pattern, the frequency of which decreases until a new stationary value is reached. The repeatability of the experiment is revealed by these two different measurements carried out under the same conditions. Moreover, different heights from which the liquid drop is released over the porous layer were tested (in the range of a few centimeters), and no significant differences between results were found.

The filling fraction of the porous layer is obtained from the extreme points of the reflectance shown in Figure 4. According to the model described above, between two measured extremes of the reflectance, the liquid advances a fixed distance in the porous layer. It is thus feasible to transform these points in a list of time-position for the liquid interface ($x$, $t$). In order to analyze the results with the model depicted by eq 6, the data must be normalized to obtain the dimensionless values ($x^*$, $t^*$). In the presented optical model, the imbibition distance $x$ is proportional to the number of extremes $N$ measured at time $t$, while the total imbibition distance $L/(1+\alpha)$ is proportional to the total number of extremes $N_T$. Taking this into account, we can calculate the dimensionless distance $x^* = x/L = N/[N_T(1+\alpha)]$. Therefore, the fitting parameters were $t_{fill}$, $\alpha$, and $N_T$.

**Ambient Pressure.** Results of capillary filling of PS layers obtained for three different ambient pressures are shown in Figure 5. In the short-time limit, the squared filling shows a linear evolution, independent of the gas pressure, in agreement with the Lucas−Washburn regime ($x \propto t^{1/2}$). As the filling fraction approaches to unity, the pressure of the gas inside the capillaries becomes important. The maximum value of the filling fraction in the limit $t^* \to \infty$ is $x^* \to 1/(1+\alpha)$, and it only depends on $\alpha$, which is proportional to the gas pressure (eq 5). The values of $\alpha$ in Figure 5 are consistent with the measured ambient pressures.

The characteristic time $t_{fill}$ is in principle independent of the gas pressure (eq 4). Accordingly, the values of $t_{fill}$ in Figure 5 are quite similar, since the experiments were carried out with the same conditions except the ambient pressure.

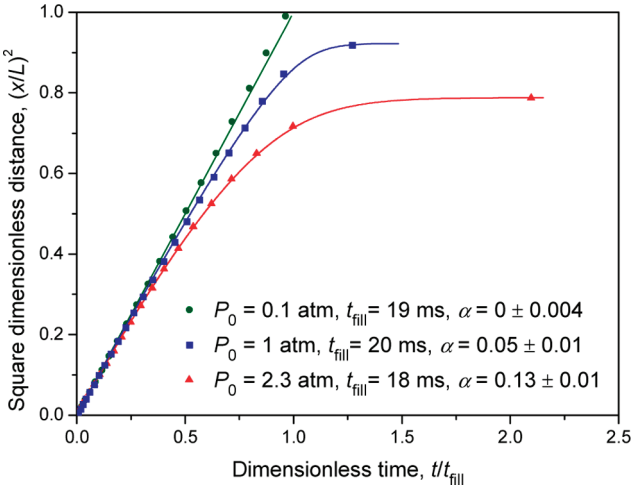


**Figure 5.** Squared filling fraction as a function of time for isopropyl alcohol in a PS layer prepared at 13 mA/cm$^2$. Symbols are the extremes of the time response reflectance (as in Figure 4) at different pressures. Lines represent the model (eq 6) with the fitting parameters $t_{fill}$ and $\alpha$ obtained for each pressure.

**Fluid Properties.** The filling dynamics of PS layers was also tested against fluid properties. Measurements of the penetration of acetone, hexane, methanol, ethanol, and isopropanol were carried out at atmospheric pressure. Following the procedure described above, $t_{fill}$ is obtained as a fitting parameter in each case. For a given PS layer, $t_{fill}$ (eq 4) only depends on the ratio $\mu/(\sigma \cos\theta)$, which characterizes fluid properties. This ratio is the inverse of the so-called penetrativity coefficient.[18] Results are shown in Figure 6, and the bulk properties $\sigma$ and $\mu$ for each liquid were taken from the literature.[24]

The good correlation between $t_{fill}$ and $\mu/(\sigma \cos\theta)$ observed in Figure 6 indicates that the simple model presented in this work describes correctly the main features of the filling process. Moreover, the linearity in Figure 6 implies that the values of the bulk penetrativity scale correctly for pore radii as small as 10 nm. According to the model, the slope of this curve only depends on the geometrical parameters of the PS layer, that is, $2\tau^2L^2/\langle r_h\rangle$. By using the measured value of $L$, it is possible to estimate the ratio $\langle r_h\rangle/\tau^2$.

On the other hand, the results in Figure 6 suggest potential applications of this technique to obtain information about the physical properties of a particular liquid. In a matter of milliseconds, and with a small volume of the liquid, the method is able to distinguish among different liquids based on variations of the factor $\mu/(\sigma \cos\theta)$. In addition, the parameter $\alpha$ can be used to further discriminate fluids, since it involves the surface tension only (eq 5).

**Pore Size.** Finally, we studied the filling dynamics as a function of pore radius. The penetration of isopropanol through PS layers fabricated at different current densities was measured at atmospheric pressure. The results of the normalized data along with the fitting curves are shown in Figure 7.

It is observed that larger values of $\alpha$ (see Table 1) are obtained for layers fabricated with bigger current densities, under the same pressure and other experimental conditions. From the definition of $\alpha$ in eq 5, and using the known values of pressure and fluid properties, it is possible to calculate the $\langle r_h^2\rangle/\langle r_h\rangle$ value for each current density. This relation can be

(24) *CRC Handbook of Chemistry and Physics*, 84th ed.; Lide, D. R., Ed.; CRC Press LLC: New York, 2003.
(25) Hunter, R. J. *Foundations of Colloid Science*; Oxford University Press: Oxford, UK, 1992; Vol. *1*.

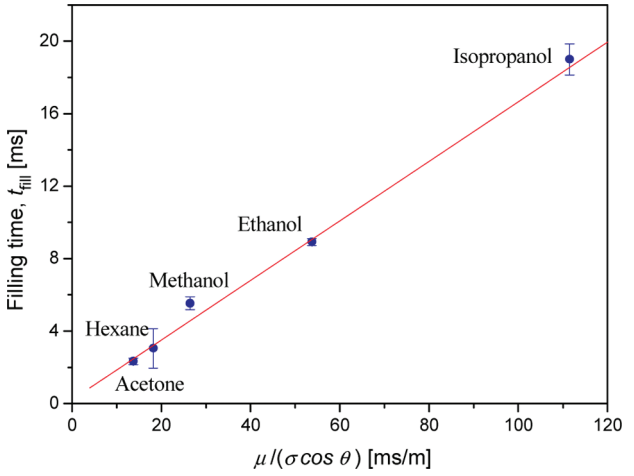


**Figure 6.** Filling time as a function of $\mu/(\sigma \cos \theta)$ for different liquids. The 15.2 $\mu$m thick PS layer utilized was fabricated using a current density of 13 mA/cm$^2$.

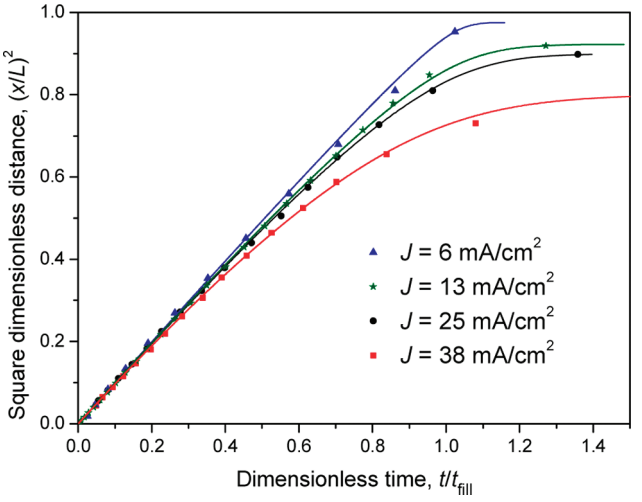


**Figure 7.** Squared filling fraction as a function of time for isopropyl alcohol at atmospheric pressure. Symbols are the extremes of the time response reflectance (as in Figure 4) for porous layers prepared at different current densities ($J$). Lines represent the model (eq 6), with the parameters reported in Table 1.

expressed in term of the variation coefficient $C_v$ as[25]

$$\frac{\langle r_h^2 \rangle}{\langle r_h \rangle} = \langle r_h \rangle (1 + C_v^2) \qquad (7)$$

where $C_v S_h/\langle r_h \rangle$ is the normalized standard deviation. Then, for a slightly dispersive distribution of pore sizes, $\langle r_h^2 \rangle/\langle r_h \rangle \approx \langle r_h \rangle$. Further information about the pore size distribution of PS layers can be extracted from SEM images with a standard software analysis. For all current densities, we obtain $C_v^2 \approx 0.1$, indicating that the studied layers have a rather narrow size distribution.

Figure 8 compares the mean hydraulic radius $\langle r_h \rangle$ obtained from SEM images with values calculated from the capillary filling experiments. The radius $\langle r_h \rangle$ obtained from SEM images was calculated as the hydraulic radius averaged with the area of each pore (see Appendix, eq A5). The values of $\langle r_h \rangle$ involved in the fluid dynamics model were calculated from the values of α reported in Table 1, by using eqs 5 and 7, with $C_v^2 = 0.1$.

It is observed in Figure 8 that PS layers have pore sizes that increase linearly with current density, as determined from both

**Table 1. Current Density and Thickness of Each PS Layer along with the Parameters Obtained by Fitting eq *6* to Experimental Data in Figure *7***

| $J$ [mA/cm$^2$] | $L$ [$\mu$m] | $t_{fill}$ [ms] | α | $\tau$ |
|---|---|---|---|---|
| 6 | 9 | 14.1 | 0.011 | 2.8 |
| 13 | 15 | 19.7 | 0.04 | 2.5 |
| 25 | 10 | 5.7 | 0.05 | 2.4 |
| 38 | 10 | 3.7 | 0.12 | 2.6 |

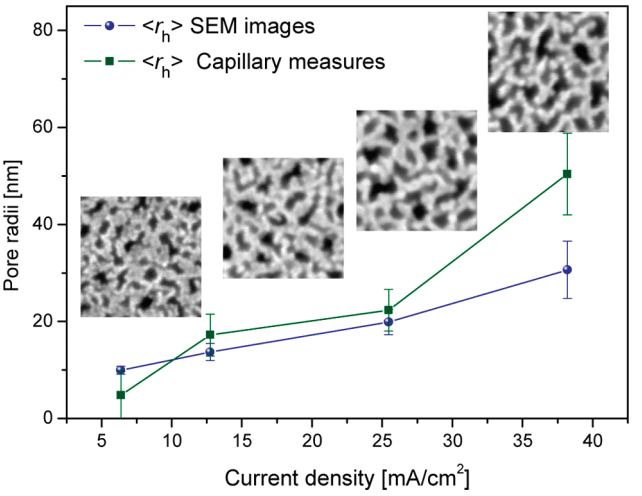


**Figure 8.** Pore radii estimated by using the fitting parameter α (eq 5) and from SEM images, for PS layers fabricated at different current densities. A 100 × 100 nm$^2$ SEM image is placed over each current density value to show the morphology of the different layers.

SEM and fluid imbibition measurements. In fact, the overall agreement between the mean pore radii obtained from each procedure is reasonably good. Only for the highest current density, where the error in the fitted α is large, the differences are statistically meaningful.

Besides, by using the values of $t_{fill}$ and $L$ in Table 1, we estimate the mean hydraulic radius over squared tortuosity $\langle r_h \rangle/\tau^2$ for each current density used. By comparing $\langle r_h \rangle/\tau^2$ to the values of $\langle r_h \rangle$ determined from SEM images, we calculate the tortuosity $\tau$ for each PS layer. The results are presented in Table 1, where one may observe that the tortuosity is approximately equal to 2.6 regardless of the current density. It is worth noting that the case of pores perfectly aligned in flow direction leads to $\tau = 1$, while isotropic orientation of pores in three dimensions ideally leads to $\tau = 3$. The values of $\tau$ obtained for PS layers indicate that, during the imbibition process, the streamlines are (locally) neither straight nor perfectly parallel to each other, as one would infer from Figure 1b.

The values of $\tau$ obtained for PS layers (Table 1) may appear rather large, given the tubular structure of the pores observed in Figure 1b (though streamlines are not expected to be well aligned in these pores). Furthermore, a closer inspection to Figure 1b shows that capillary surfaces present a certain degree of roughness, which can significantly reduce the effective hydrodynamic radius and hence the filling speed.[26] In what follows, we discuss this potential effect as an alternative approach to the concept of tortuosity.

If one considers perfectly straight capillaries ($\tau = 1$) presenting surface roughness with a characteristic size $\delta$, as a first approximation

(26) Stukan, M. R.; Ligneul, P.; Crawshaw, J. P.; Boek, E. S. *Langmuir* **2010**, *26*, 13342.

the effective hydrodynamic radius can be written $r_e = r - \delta$, where $r$ is the nominal capillary radius (say the one obtained from SEM, as a reference). Besides, the possible existence of a stagnant layer of adsorbed liquid molecules on the capillary surface also reduces the effective radius, as described in ref 8. Under these conditions, the filling time results $t_{fill} = 2\mu L^2/[r\sigma \cos\theta(1 - \delta/r)^2]$. Matching this expression to eq 4 yields $\tau^2 = (1 - \delta/r)^{-2}$. Therefore, if the numerical factor $\tau^2 \approx 6.8$ obtained above is now completely attributed to surface roughness, one obtains $\delta/r \approx 0.6$ for all the PS layers studied here. This value also appears rather large, but it is not unreasonable taking into account the aspect of capillaries observed in SEM images (Figure 1b).

The overall result is that the intrinsic nanoscopic features of the porous matrix lead to a considerable reduction of the filling speed, in relation to the values predicted with the pore radius obtained from SEM. From the point of view of the fluid dynamics model, the effect is condensed in a factor $\tau^2$, or alternatively $(1 - \delta/r)^{-2}$, entering the characteristic time $t_{fill}$. Thus, the reduction of the filling speed may be entirely attributed to the tortuosity of the pores on the one hand or to a reduced effective radius on the other, while the actual situation surely involves a combination of both effects.

## Conclusions

A novel method to measure capillary filling in nanostructured porous silicon membranes is presented, which is based on laser interferometry. The experimental technique is relatively simple to implement and yields highly reproducible data, measurements take a few milliseconds, and sample volumes consumed are in the order of microliters.

We propose a simple model for the capillary filling dynamics which appropriately represents experimental data in the whole range of measured time. The only unknown parameters of the model are the average hydraulic radius and the tortuosity of the pores. Once these parameters are characterized by fitting the model to experimental data, the method can be readily used to determine fluid properties such as viscosity and surface tension. On the other hand, by using a known liquid, from imbibition measurements we can obtain information of the porous layer morphology (size and tortuosity). It is worth remarking that the average hydraulic radius thus obtained quantitatively agrees with measurements made by SEM images.

One may finally conclude that the employment of this method (involving both the experimental technique and the fluid dynamic model) in nanofluidic applications is a promising strategy that deserves further research.

**Acknowledgment.** We acknowledge the technical support of Ramón Saavedra. This work was financed by CONICET (Grants PIP 5730 and PIP 0317), ANPCyT (Grant PICT 32515), and UNL (CAI+D 12G/328).

## Appendix A

Here we describe a simple way to extend the fluid dynamics model of a single capillary (eq 1) to the PS film. In fact, a collection of capillaries is considered, which is characterized by an average hydraulic radius and a particular tortuosity. Taking into account that different capillary geometries are present, the flow rate of the fluid through the porous film can be expressed as

$$Q = \sum_i n_i v_i A_i \tag{A1}$$

where $n_i$ is the number of pores with cross-sectional area $A_i$ and fluid velocity $v_i$. The fluid velocity in each single pore can be included according to eq 1, with effective values of the length $L_{eff}$. One may further introduce the tortuosity $\tau$, which is defined as the ratio of the actual distance traveled by the fluid in the twisted path of the pores, to the distance traveled in $x$ direction, that is, $\tau = L_{eff}/L = x_{eff}/x$. In addition, to account for different pore geometries, the radius $r$ in eq 1 has to be replaced by the hydraulic radius $r_{h,i} = 2A_i/P_i$.[21] Therefore, eq A1 results

$$Q = \frac{1}{8\mu\tau^2 x}\left(2\sigma\cos\theta\sum_i n_i r_{h,i} A_i - p_0\frac{x}{L-x}\sum_i n_i r_{h,i}^2 A_i\right) \tag{A2}$$

Concerning Laplace pressure, this approach implicitly assumes that menisci present a unitary radius of curvature given by $r_{h,i}/\cos\theta$ and that $\theta$ is independent of capillary geometry. In the term corresponding to air compression, $p_0$ is allowed to be the same for all capillaries, taking into account that pores are somehow interconnected in the actual porous matrix.

During the filling process, we observe that the fluid advances in a flat front with the velocity $dx/dt$ (see Figure 3), which is measured in the experiment over a wide cross-sectional area of the film. Consequently, mass conservation indicates that the macroscopic flow rate can be also expressed

$$Q = \frac{dx}{dt}\sum_i n_i A_i \tag{A3}$$

Eliminating $Q$ from eqs A2 and A3 yields the following expression for the measured fluid velocity

$$\frac{dx}{dt} = \frac{1}{2\mu\tau^2 x}\left(\sigma\cos\theta\frac{\sum_i n_i r_{h,i} A_i}{\sum_i n_i A_i} - p_0\frac{x}{L-x}\frac{\sum_i n_i r_{h,i}^2 A_i}{\sum_i n_i A_i}\right) \tag{A4}$$

which is exactly eq 2 with the following definitions

$$\langle r_h\rangle = \frac{\sum_i n_i r_{h,i} A_i}{\sum_i n_i A_i} = \frac{2\sum_i n_i A_i^2/P_i}{\sum_i n_i A_i} \tag{A5}$$

$$\langle r_h^2\rangle = \frac{\sum_i n_i r_{h,i}^2 A_i}{\sum_i n_i A_i} = \frac{4\sum_i n_i A_i^3/P_i^2}{\sum_i n_i A_i} \tag{A6}$$

These expressions are also useful to determine the average hydraulic radius from SEM images, where the $P_i$ and $A_i$ of a statistically meaningful number of pores can be extracted using a standard image tool software.